Title

Securing the Payload, Finding the Cell, and Avoiding the Endosome: Peptide-Targeted, Fusogenic Porous Silicon Nanoparticles for Delivery of siRNA

Permalink

https://escholarship.org/uc/item/7hw3z8gt

Authors

Kim, Byungji
Sun, Si
Varner, Judith A
et al.

Peer reviewed

Securing the Payload, Finding the Cell, Avoiding the Endosome: Peptide-Targeted, Fusogenic Porous Silicon Nanoparticles for Delivery of siRNA

Byungji Kim,

Materials Science and Engineering Program, University of California, San Diego, 9500 Gilman Dr., La Jolla, CA 92093, USA

Si Sun,

Department of Obstetrics and Gynecology, Union Hospital, Tongji Medical College, Huazhong University of Science and Technology, Wuhan 430022, China

Judith A. Varner,

Moores Cancer Center and Department of Pathology, University of California, San Diego, La Jolla, CA, USA

Stephen B. Howell,

Moores Cancer Center and Department of Medicine, University of California, San Diego, La Jolla, CA, USA

Erkki Ruoslahti,

Cancer Research Center, Sanford Burnham Prebys Medical Discovery Institute, La Jolla, California 92037, USA; Center for Nanomedicine and Department of Cell, Molecular and Developmental Biology, University of California, Santa Barbara, Santa Barbara, California 93106-9610, USA

Michael J. Sailor

Materials Science and Engineering Program, University of California, San Diego, 9500 Gilman Dr., La Jolla, CA 92093, USA; Department of Chemistry and Biochemistry, University of California, San Diego, 9500 Gilman Dr., La Jolla, CA 92093, USA

Abstract

Despite the promise of RNAi therapeutics, the delivery of oligonucleotides selectively to diseased tissues in the body, and specifically to the cellular location in the tissues needed to provide optimal therapeutic outcome, remains a significant challenge. Here, key material properties and biological mechanisms for delivery of siRNAs to effectively silence target-specific cells *in vivo* are identified. Using porous silicon nanoparticles as the siRNA host, tumor-targeting peptides for selective tissue homing, and fusogenic lipid coatings to induce fusion with the plasma membrane, we show that the uptake mechanism can be engineered to be independent of common receptor-mediated endocytosis pathways. Two examples of the potential broad clinical applicability of this

*
msailor@ucsd.edu.

concept in a mouse xenograft model of ovarian cancer peritoneal carcinomatosis are provided: silencing the *Rev3l* subunit of polymerase Pol ζ to impair DNA repair in combination with cisplatin; and reprogramming tumor-associated macrophages into a pro-inflammatory state.

Graphical Abstract

Fusogenic porous silicon nanoparticles enable RNAi therapeutics by effectively delivering its siRNA payload to selectively targeted cells *in vivo* to induce significant gene silencing. The fusogenic particles offer a generalizable platform technology that can be modified in a facile manner into different formulations; two model therapeutics (gene therapy and immunotherapy) are demonstrated to treat ovarian cancer.
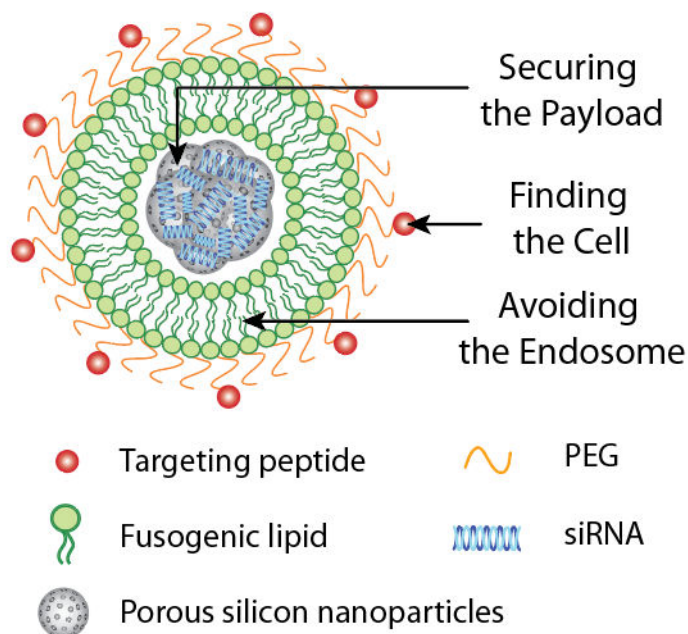
Keywords

Immunotherapy; Ovarian Cancer; Liposome; Macrophage

1. Introduction

Of the ~100 FDA-approved anticancer drugs, about 40% are cytotoxic agents and 60% are inhibitors of oncogenic pathways[1]. As the discovery of key oncogenic markers and pathways has progressed, siRNAs have emerged as a promising class of drugs to transiently silence oncogenic mutations. Despite the worldwide effort expended in the development of siRNA-based therapeutics over more than 15 years, substantial challenges have limited their clinical translation. The first siRNA-based drug was approved only in the last year, and that only for treatment of a rare hereditary disease[2]; there is currently no approved cancer therapeutic based on siRNA. A primary obstacle in this endeavor has been the lack of

delivery vehicles that can overcome *in vivo* clearance and cellular degradation via endocytosis[3, 4].

One of the early proposed solutions to the problem of endocytotic sequestration and subsequent lysosomal degradation of siRNA was delivery *via* fusogenic liposomes[5]. Fusogenic liposomes directly fuse with the cell membrane, bypassing endocytotic uptake pathways[6]. While they have shown promise as delivery vehicles for RNAi therapeutics[7], liposomes suffer from a generally low carrying capacity for nucleic acid therapeutics[8] and leakage of their payloads either during storage or *in vivo*[9]. We recently demonstrated a delivery system that harnessed together a fusogenic lipid and a solid porous silicon nanoparticle (pSiNP) core. The system capitalized on the relatively high loading of siRNA[10] into pSiNPs that can be accomplished via a calcium ion precipitation strategy[11] that stabilizes the siRNA payload and minimizes leakage. When grafted with the appropriate homing peptide, the fusogenic nanoparticles (FNPs) showed a strong *in vivo* gene silencing effect specific to macrophages[8]. Here, we evaluate the mechanism of action of the FNPs, and conclude that it is generalizable to other cell types, provided the targeting peptide is sufficiently specific. We then validate its clinical applicability as a platform technology by demonstrating the activity of two separate siRNA therapeutics against ovarian cancer peritoneal carcinomatosis, intercepting two very different oncogenic pathways: (1) a cancer cell-targeting fusogenic nanoparticle (C-FNP) that sensitizes cells to platinum (Pt)-based chemotherapy by suppressing their DNA repair machinery; and (2) a tumor-associated macrophage (TAM)-targeting fusogenic nanoparticle (T-FNP) that reprograms the immune system to enhance T-cell infiltration and downregulate immunosuppression.

2. Results and Discussion

2.1. Structure and composition of fusogenic nanoparticles (FNPs)

The FNPs (Figure 1a) consisted of a porous silicon nanoparticle core loaded with siRNA (pSiNP), and a fusogenic lipid coating decorated with pendant targeting peptides. The porous silicon nanoparticle cores were prepared by electrochemical etch of silicon wafers, and the siRNA payload was loaded into the nanoparticle with the assistance of calcium ion as previously described[11, 12]. The calcium ion serves two functions in this preparation. First, it acts to neutralize the negative charge of the silicon oxide surface of the pSiNP and the negative charge of the nucleic acid[13], in a role similar to that played by the cationic polymers or lipids commonly deployed in nucleic acid delivery systems[7, 14]. Second, partial dissolution of the silicon skeleton during the loading procedure generates silicic acid that then forms a precipitate with Ca (II) ions, generating a calcium silicate phase that effectively seals the nanostructure and traps the nucleic acid payload[11]. This sealing chemistry is remarkably efficient in that it can load up to 25% nucleic acid by mass; in the present case the mass loading of siRNA was 10% (defined as mass of siRNA loaded relative to mass of siRNA-containing nanoparticle). Figure S1 shows the transmission electron microscope (TEM) images of the pSiNPs before (Figure S1a) and after (Figure S1b) siRNA loading with the calcium sealing method; the pSiNPs before loading show open and empty pore structures, whereas the pSiNPs after calcium sealing show closed pores with a dense coating around the pSiNP skeleton. The nanoparticle was then coated with the fusogenic

lipid coating and the targeting peptide of interest was coupled to the PEG component of this coat *via* a terminal maleimide group; for non-targeted particles we used PEG with a methoxy terminus (mPEG). The overall hydrodynamic diameter of the resulting FNPs was 170 nm, and the zeta potential was +9 mV when mPEG was used. For the formulations that contained a peptide targeting group, the zeta potential was closer to neutral (Table S1). The siRNA-loaded particles were stable when stored at -80°C for > 1 month with no loss of functionality[12].

2.2. Factors favoring cellular membrane fusion vs. endocytosis

The lipids that comprised the fusogenic coating were selected based on the known ability of liposomes with the composition used to fuse with the cellular membrane and avoid endocytosis[7, 8, 15]; we assumed that the composition would behave similarly if the final liposomal construct contained a core of solid nanoparticles. Each lipid component plays a role in plasma membrane fusion (Table S2)[8]. First, DMPC is the major structural component, with a phase transition temperature (24°C) below the physiological temperature (37°C). This property allows the lipids to be in a fluidic liquid crystal phase (L_α) *in vivo*, which is the phase to which endogenous extracellular vesicles transition when fusing[16]. We selected DSPC (T_{ph}= 55°C) and DLPC (T_{ph}= -2°C) as alternative lipids to test for the importance of lipid phase in the fusion process. Second, cationic DOTAP serves to attract the negatively charged plasma membrane; another widely used cationic lipid, DOTMA, was selected as an alternative. The key difference is that, while DOTAP becomes completely protonated and more cationic at the physiologic pH of 7.4, DOTMA does not[16]. Finally, polyethylene glycol (PEG) is hypothesized to interact with cellular surface proteins in a manner akin to the endogenous SNARE proteins[17]. To test the influence of the PEG component, one alternative test formulation contained no PEGylated lipid.

The above formulations were used to probe the mechanism of cellular uptake *in vitro*, using CAOV-3 human ovarian adenocarcinoma cells. For these tests we used a methoxy group rather than a specific targeting peptide conjugated to the PEGylated lipid component. Figures 1b–f show confocal images of CAOV-3 cells treated with FNPs or with the alternative lipid compositions. When loaded with the lipophilic DiI fluorophore as a stain for the lipid membrane, FNPs demonstrated fusion and transfer of DiI into the plasma membrane (Figure 1b). When the cells were stained with LysoTracker Green, we observed minimal co-localization between the DiI lipid stain and the lysosomes (Pearson's correlation coefficient, or PCC = 0.08), indicating that the FNPs did not undergo endocytosis. However, when we replaced the DMPC component with DSPC (which has a higher T_{ph} and is in the L_β gel phase at 37°C), we observed endocytosis and co-localization between the lysosomes and the lipid stain (PCC= 0.51; Figure 1c). On the other hand, when DLPC (which has lower T_{ph} and is in the L_α liquid crystalline phase at 37°C) was used, we observed an overall lower level of DiI loading into the particle coating (data not shown). This result can be ascribed to the lower stability of the particles, as the DLPC lipids are expected to remain in a more fluidic state at during particle synthesis and at physiologic temperature due to their low phase transition temperature (T_{ph}= -2°C). Despite the lower degree of dye loading, membrane fusion was still observed, although the formulation showed substantial co-localization between the lysosomes and the lipid stain compared with the FNP formulation

(PCC=0.20; Figure 1d). Taken together, the data indicate that the fluidity of the lipid is important for effective membrane fusion; if the lipid is in the more rigid gel phase it is readily endocytosed and if it is in a more fluid state the entire construct is less stable during synthesis.

Next, we observed the uptake of particles where DOTAP was replaced by DOTMA. Due to the decrease in degree of protonation of the lipid, the overall zeta potential of the final particle was less positive. As a result, there was a marked reduction in particle uptake, although the particles that were taken up underwent fusion, as determined by the relatively low degree of co-localization observed between the lysosomes and the lipid stain (PCC= 0.14; Figure 1e). Thus, consistent with much prior work, the higher positive charge facilitates uptake and fusion due to the electrostatic attraction between the cationic FNPs and the anionic plasma membrane[18].

Finally, the formulation lacking DSPE-PEG was observed to have a high degree of co-localization between the lysosomes and the lipid stain suggesting extensive endocytosis (PCC=0.46; Figure 1f). As has been described previously for PEGylated nanoparticles and akin to the endogenous SNARE mechanism[17], the data are consistent with the hypothesis that PEG assists in dehydrating the gap between the fusogenic lipid coating on the nanoparticle and the plasma membrane on the cell, making lipid fusion energetically and structurally favorable.

From the above studies we can conclude that there are at least three factors favoring fusion of the FNPs with the plasma membrane: (1) a substantial portion (>70% molar ratio) of the composition must have a moderately low phase transition point near room temperature; (2) the overall zeta potential of the lipid composition must be cationic (~10 mV); and (3) PEG or an equivalent dehydrating agent must be present in the lipid formulation.

2.3. Cellular uptake of FNPs

We next investigated the impact of inhibition of the major endocytic pathway mediators[3] — caveolin (*Cav1*), clathrin (*Cltc*), and macropinocytosis (*Rac1*) — on cellular uptake of FNPs (Figure S6, **pathway #1**). The degree of uptake of the FNPs was compared to a non-fusogenic nanoparticle construct (NNPs; identical structure as FNPs, but with a lipid coating that is not fusogenic, see Methods section). The data are shown in Figure 2a and the corresponding confocal images are shown in Figure S2. For all three markers, we found that while non-fusogenic nanoparticles showed a significant decrease in uptake, the fusogenic nanoparticles were taken up at levels equivalent to the non-transfected control, and at significantly higher quantities than the NNPs (paired t-test; p= 0.024 (*Cav1*); = 0.031 (*Cltc*); and = 0.002 (*Rac1*)). Thus, we conclude that fusogenic FNPs are taken up *via* pathways that are independent of endocytosis.

In order to determine whether specific biological markers and pathways exert influence on the fusogenic uptake of the FNPs, the effect of disabling other proteins that play important roles in cellular uptake and metabolism of lipids were studied (Figure S6). A summary of the pathways investigated is given in the table shown in Figure S6, and the detailed results are discussed in the Supplementary Results and Discussion. Overall, we observed that FNPs

were able to undergo fusogenic uptake in a manner independent of the major known endocytosis or vesicle traffic pathways, but their uptake was highly dependent on mediators of intracellular vesicle fusion. It should be stressed that these results remain primarily phenomenological, because while the biological mechanism of these proteins on a molecular scale are elucidated (*e.g.* SNARE protein interaction), the interactions between the selected pathways and lipid dynamics are not known at this time, and there may be additional cellular uptake pathways as yet unidentified. However the data clearly show that the FNPs enter the cell in a manner that bypasses endocytosis.

2.4. Intracellular fate of FNP components

We evaluated the fate of the three major components of the FNP platform: (1) the fusogenic lipid coating; (2) the porous silicon nanoparticles in the core; and (3) the siRNA payload. We started with the hypothesis that the particles dissolve and release their siRNA payload upon shedding their lipid coats. When immersed in PBS solution, calcium silicate-coated pSiNPs are vulnerable to dissolution, releasing their payload and generating silicic acid as a degradation product[19]. This dissolution reaction is faster in PBS buffer solution than it is in pure (deionized) water, and the rate of dissolution roughly scales with increasing surface area to volume ratio[20] of the particles. The pSiNPs in the present study behaved similarly; nanoparticles that lacked a lipid coating (pSiNPs) dissolved and released 70% of their siRNA payload within the first 30 min of incubation in PBS at 37°C, which increased to 90% after 6h of incubation (Figure 2b). In contrast, the lipid-coated nanoparticles (either FNPs or NNPs) released very little (5%) siRNA in the first 30 min, and only 25% was released in 24 h. The particles released ~75% of their total siRNA payload after 168 h (7 days) of incubation, a factor of >300 fold slower than what was observed for the particles without a lipid coat. Complete release from the lipid-coated nanoparticles was achieved by 336 h (14 days). Thus, the lipid coating substantially impedes porous silicon dissolution and siRNA release under physiological conditions. This is a striking result considering the substantial leakage that is typically observed from conventional liposomal formulations that contain an aqueous core[21], and illustrates the advantage of locking the otherwise highly soluble siRNA payload into a solid core[22].

We next tracked the intracellular fate of the components, using CAOV-3 cells in a series of *in vitro* experiments. Cells were treated with DiO-loaded fusogenic (FNP; Figure 2c) or non-fusogenic (NNP; Figure 2d) lipid-coated pSiNPs that contained an siRNA payload. DiO is a lipophilic green fluorescent dye, used here to track the lipid component of the FNPs, and the siRNA was tracked with a pendant red Cy3 tag. The pSiNPs were tracked using their intrinsic red to NIR photoluminescence, which derives from quantum-confined silicon[23]. This provided a direct measure of the extent of dissolution of the silicon nano-carrier, as the photoluminescence disappears when the nanoparticles dissolve[24]. The FNPs showed clear dispersion of the Cy3-tagged siRNA in the cell cytosol post-fusion, whereas the DiO affiliated with the lipid components was retained in the cell membrane (Figure 2c). A similar experiment was performed using an siRNA payload without the red Cy3 tag and monitoring the red emission from the pSiNPs. Signals from the pSiNPs, readily observable in cell-free media, were not visible after fusion with the cells (Figure 2c). This indicates that the nano-carrier was rapidly degraded upon encounter with the cells, presumably a result of shedding

of its fusogenic lipid coating. In contrast, signals from the pSiNPs were prominent in cells treated with non-fusogenic NNPs (Figure 2d), which enter the cell *via* endocytosis. The non-fusogenic NNPs showed strong co-localization of the red pSiNP signal with the DiO signal from the lipid, indicating that the lipid coat around the pSiNPs was retained upon endocytosis (Figure 2d). In separate experiments the DiO signal was found to co-localize with the Cy3 signal from a suitably labeled siRNA payload, showing that the endocytosed NNPs were not able to release the siRNA payload into the cytosol. These data indicate successful sequestration of the siRNA and pSiNPs within the liposomes, and support the mechanism proposed in Figure 1a, in which the fusogenic coating is shed upon encounter with the cell membrane, and the pSiNPs carrying their siRNA payload are delivered directly into the cellular cytoplasm. Once they lose their protective lipid coating, the pSiNPs dissolve rapidly, releasing their siRNA payload. When a non-fusogenic coating is used, the particles become endocytosed, which permits the lipid coat to remain intact and prevents pSiNP degradation and siRNA release. Thus, the conditional shedding of the lipid coating around the pSiNP core *via* fusogenic uptake is critical to cytosolic release of siRNA.

2.5. In vitro validation of FNPs for therapeutic applications

In order to evaluate whether or not the FNPs offer a generalizable solution for siRNA therapies, we evaluated two different approaches (Figure 3a): a chemosensitizing siRNA (C-FNPs) that inhibits the DNA repair mechanism in cancer cells, and an immunosuppressing siRNA (T-FNPs) that reprograms tumor-associated macrophages to enhance the immune system's ability to clear these aberrant cells. We selected the first therapeutic (C-FNPs) to sensitize cancer cells to cisplatin, as Pt-resistant or Pt-refractory ovarian cancer is seen in over 70% of patients at advanced stages; chemoresistant tumors cause high morbidity, and has been an unsolved problem for over two decades[25, 26]. Cisplatin crosslinks cellular DNA which trigger apoptosis in the absence of adequate DNA repair[27]. Cancer cells that can repair the modified DNA well exhibit chemoresistance[26, 28]. While key predictors of Pt-drug response have been identified[26, 28], there is no preventative measure against the development of resistance, or reliable strategy to induce chemosensitivity. To this end, we chose to deliver siRNA against *Rev3l* (subunit of DNA repair polymerase, Pol ζ) to disable a component of the DNA repair pathway known to enhance chemosensitivity in the CAOV-3 human ovarian adenocarcinoma[29]. For this model we specifically targeted the FNPs to ovarian cancer cells using the iRGD peptide (Table S3)[30].

The second therapeutic tested (T-FNPs) was designed to reprogram tumor-associated macrophages (TAMs) to inhibit their oncogenic pathways[31]. PI3kγ is a key regulator of immunosuppression, and its downregulation has shown benefits in increasing both CD8+ T-cell recruitment to the tumor and sensitivity of immunosuppressive myeloid cells to checkpoint inhibitors[32]. In order to target TAMs selectively, we used the LyP-1 peptide (Table S3), which homes to TAMs and tumor-associated lymphatic vessels[33, 34]. The LyP-1-conjugated FNPs were loaded with siRNA against *Pi3kγ*, with the goal of eliciting tumoricidal behavior in TAMs.

First, we verified that FNPs retained their fusogenic nature after conjugation with targeting peptides (Figure 3b). For both CAOV-3 cancer cells and J774a.1 macrophages, FNPs

without targeting peptides successfully fused with the plasma membrane. In CAOV-3 cells treated with iRGD-conjugated, DiI-loaded nanoparticles (C-FNPs), we saw uniform distribution of the DiI signals on the cell plasma membrane indicating successful fusion, and the FAM-tagged iRGD peptides segregated into the cytoplasm. We saw the same trend in J774a.1 cells when the LyP-1-conjugated, DiI-loaded nanoparticles (T-FNPs) were used, indicative of successful fusion to this macrophage cell line. The insertion of the iRGD or LyP-1 targeting peptides into the cytosol of their respectively targeted cells is consistent with the established CendR mechanism[35] where the peptide initially binds to the target receptor to undergo peptide cleavage, then transfers to a secondary receptor to undergo receptor-mediated endocytosis (Table S3)[34, 35, 36]. In some of the cells, co-localization between the DiI and the FAM-LyP-1 peptides on the plasma membrane was observed, suggestive of the intermediate stage prior to migration of the peptide to its secondary receptor. Based on these results, we believe that fusion occurs immediately after the peptide binds to its primary cellular receptor, and that by the time the peptide transfers to its secondary receptor, fusogenic uptake has occurred. This hypothesis is further supported by experiments with non-fusogenic constructs; in that case both C-NNPs and T-NNPs were endocytosed, and their DiI and FAM-peptide signals were strongly co-localized within the cell cytoplasm. Additionally, the successful fusion to the J774a.1 cells by FNPs are significant, as macrophages are highly phagocytic compared to other cell types. We observed that macrophages induced a faster fusogenic uptake at a rate that was approximately three-times faster than that of CAOV-3 cells. Overall, the FNPs retain their ability to fuse with cellular membranes even when a cell-specific targeting peptide is deployed on the exterior of the nanoparticle's lipid membrane.

Next, we determined the efficiency of knockdown of the *Rev3l* gene target in CAOV-3 cancer cells (Figure 3c) that could be achieved using the cancer cell-targeting iRGD peptide. Both fusogenic and non-fusogenic nanoparticles (C-FNPs and C-NNPs) were compared. We serially diluted the siRNA dose starting from a maximum dose of 100 nM, based on previous work (FNPs attained >95% relative knockdown efficiency in RAW264.7 macrophages at this concentration of siRNA)[8]. The dose-response curve for C-FNPs was similar to that of Lipofectamine (Lf), and over 90% knockdown efficiency was attained with a dose of 50 nM siRNA. In contrast, C-NNPs reached a plateau of only ~50% knockdown efficiency under similar conditions.

We next compared the efficiency of silencing of *Pi3kγ* in J774a.1 cells (Figure 3d), using the macrophage-targeting LyP-1 peptide on the fusogenic or non-fusogenic nanoparticles (T-FNPs or T-NNPs). Based on the above results from the cancer cell studies, we selected 50 and 100 nM siRNA doses. When the fusogenic T-FNPs were used, both 50 nM and 100 nM doses were able to induce significantly higher knockdown of *Pi3kγ* compared with the non-fusogenic T-NNPs (p <0.01) or with Lipofectamine (p<0.05), based on One-way ANOVA ([$F_{(6, 36)}$=113.6, p=1.9×10^{-21}]) and Tukey HSD test. Although J774a.1 is a difficult cell line to transfect[37], T-FNPs were able to attain approximately 75% knockdown efficiency at 50 nM of siRNA, and 85% at 100 nM of siRNA.

The chemosensitizing effect of the *Rev3l* siRNA payload was evaluated using the C-FNPs. We pre-transfected the CAOV-3 tumor cells with siREV3L formulations, then treated the

cells with increasing concentrations of cisplatin (cDDP; 0–100 μg/mL). Figure 3e shows the dose-response curve of cDDP in transfected cells, and Figure S7 shows the IC_{50} values quantified from the dose-response data. While the IC_{50} of cDDP in cells treated with PBS or sham siRNA-loaded C-FNP (C-FNP/siLuc) were 72.1 μg/mL and 74.9 μg/mL, respectively, the IC_{50} in non-fusogenic C-NNP and Lipofectamine (Lf) treatments decreased to 54 μg/mL and 50.6 μg/mL, respectively. However, C-FNPs induced a greater increase in cDDP-sensitivity, with IC_{50} of only 29.9 μg/mL, which was significantly lower than all other transfectant groups ($p < 0.004$). Thus, transfection with 50 nM siREV3L using C-FNPs was able to increase the susceptibility of CAOV-3 cells to a dose of cDDP that was more than two-fold lower than what was needed in the absence of *Rev3l* silencing.

2.6. Biosafety, biodistribution, and selective targeting of FNPs

Prior to therapeutic application, we verified the biosafety of C- and T-FNPs. Figures S8a and b show cytotoxicity assays of the formulations in CAOV-3 and J774a.1 cells, respectively. At an siRNA dose of 50 nM, neither the targeting peptide-conjugated FNPs nor the siRNA against *Rev3l* and *Pi3kγ* induced any *in vitro* cytotoxicity. Moreover, hematoxylin and eosin (H&E) stains of the major organs in healthy mice intravenously injected with T-FNPs or C-FNPs showed normal morphology and no lesions (Figure S9).

Next, we looked at biodistribution of the FNPs in a mouse model of peritoneal carcinomatosis, established by intraperitoneal (IP) injection of CAOV-3 human ovarian adenocarcinoma cells in 6–8 week old female athymic nude mice. We allowed the tumor nodules grow for 3 weeks, then IP injected PBS, non-conjugated FNPs, T-FNPs, or C-FNPs loaded with lipophilic DiI. At 1h and 24h post-injection, we harvested the major organs and selected tumor nodules of similar size, approximately 100 mm^3. For animals where tumor nodules were smaller than 100 mm^3, the largest nodules were selected. The tissues were assayed for DiI signal localizations. Fluorescence imaging revealed that the DiI-loaded particles were localized primarily in the tumor nodules regardless of the accumulation time (Figure 4a, b). Both T-FNPs and C-FNPs showed significant increase in tumor accumulation from 1 h to 24 h ($p < 0.01$ for T-FNPs; $p < 0.05$ for C-FNPs), and both formulations accumulated in the tumor more effectively than the PBS and non-targeted FNP groups ($p < 0.05$ for T-FNPs; $p < 0.01$ for C-FNPs).

A second mouse model was established as a xenograft tumor model by subcutaneously injecting CAOV-3 cells with matrigel. As the CAOV-3 line has difficulty forming xenografts, tumor masses were <15 mm^3 in size[38]. When the therapeutic formulations were intravenously injected, a similar biodistribution trend was seen in the xenograft model as was seen with the local IP injection in peritoneal carcinomatosis model: primary accumulation in tumors, increased DiI accumulation from 1 h to 24 h of circulation, and superior tumor homing by T- and C-FNPs compared to non-targeted FNPs (Figure S10).

Flow cytometry was used to quantify cell-specificity of T- and C-FNPs. We IP injected PBS, non-targeted FNPs, T-FNPs, C-FNPs, and a 50:50 cocktail of C- and T-FNPs, and waited 24 h prior to sample collection. Immune cells were collected by intraperitoneal lavage and the tumor nodules were harvested and homogenized. Macrophages from both the lavage and homogenized tumor nodules were eluted by magnetic separation using Anti-F4/80 beads.

The purified macrophages (Figure 4c–f) and the homogenized tumor nodules (after extraction of macrophages, Figure 4g–j) were subjected to flow cytometry analysis, detecting the DiI signal channel. The non-targeted FNPs showed minimal homing to either macrophages (4.19%; Figure 4c) or tumor cells (1.13%; Figure 4g). In contrast, the T-FNPs (which deployed the TAM-homing LyP-1 peptide) successfully homed to macrophages (21.40%; Figure 4d) and not to the macrophage-free tumor nodule cells (0.01%; Figure 4h). Conversely, C-FNPs (which deployed the tumor cell-homing iRGD peptide) did not bind to macrophages (0.00%; Figure 4e) while it strongly accumulated in tumor cells (6.79%; Figure 4i). When co-injected, the T-FNPs and C-FNPs homed to both macrophages (29.6%; Figure 4f) and tumor nodules (11.2%; Figure 4j). Observing the FAM signal channel on FAM-conjugated targeting peptides showed a similar trend of selective targeting (Figure S11), and the accumulation ratios are reported in Table S4. Thus, we confirmed that pendant homing peptides can effectively target FNPs to their intended cells.

2.7. *In vivo* therapeutic efficacy of FNPs

With the ability of the peptide-conjugated FNPs to selectively target cells *in vivo* established, we next evaluated if FNPs could induce significant gene silencing *in vivo*. After 3 weeks of tumor growth, we IP injected PBS, T-FNPs, or C-FNPs. After 24 h, we quantified gene expression using the quantitative reverse transcription polymerase chain reaction (qRT-PCR) on macrophages and tumor cells (Figs 5a and b).

The TAM-targeting T-FNPs loaded with siRNA against *Pi3kγ* were able to induce 81% knockdown efficiency in the macrophages (purified from both the peritoneal lavage and tumor homogenates), while the chemo-sensitizing C-FNPs loaded with siRNA against *Rev3l* had no effect (Figure 5a). Conversely, in tumor cells the C-FNPs induced a silencing efficiency for *Rev3l* expression by 76%, while T-FNPs showed no effect (Figure 5b). Thus, only targeted FNPs with siRNA appropriate for the cell type were able to induce a potent *in vivo* gene silencing effect, and there were no detectable off-target acute toxicities.

Lastly, we conducted combination therapy experiments using cisplatin (cDDP) with: (1) immunotherapy by reprogramming macrophages to their tumoricidal phenotype (using T-FNPs); and (2) gene therapy by sensitizing cancer cells to cDDP (using C-FNPs). A week after IP tumor innoculation, we IP injected PBS, cDDP at 2 mg/kg, a cocktail of cDDP and T-FNPs, a co-injection of cDDP and C-FNPs, or a co-injection of cDDP, T-FNPs, and C-FNPs. Cisplatin was injected once every three days at the 2 mg/kg dose, and the T- and C-FNP formulations were injected once a week, based on literature protocols[39].

After 30 days of treatment, Figure 5c shows that while cDDP treatment alone was able to reduce the tumor nodule count by half, the difference was not statistically significant from the PBS control. However, combination treatment of cDDP with T-FNPs, cDDP with C-FNPs, and all three together (cDDP with T-FNPs and C-FNPs) significantly reduced the total number of tumor nodules (One-way ANOVA, [$F_{(4,30)}=64.7$, $p=2.5\times10^{-14}$], Tukey's HSD $p<0.05$. In particular, the group given cDDP with both T-FNPs and C-FNPs was significantly more effective than cDDP with only C-FNPs ($p=0.019$), and showed a notable trend compared with the cDDP and T-FNP group ($p=0.051$). Size distribution of tumor nodules showed similar findings (Figure 5d). While the PBS control group had a wide size

distribution range of nodules from 1.3–9.4 mm, we saw a small decrease with the cDDP-only treatment group (2.2–7.4 mm), and a greater decrease in the groups given either cDDP + T-FNP (1.3–4.4 mm), or cDDP + C-FNP (1.4–6.2 mm). Remarkably, the triple combination (cDDP + T-FNP + C-FNP) produced complete elimination of detectable tumors in 6 of the 7 members of the treatment group; the seventh member of this group had only a single nodule with a size of 2.8 mm.

The above results demonstrated the utility of the FNP platform for siRNA-based treatment-- in the form of immunotherapy and gene therapy. They further showed that combination therapy to target multiple aspects of cancer can yield an improved therapeutic outcome relative to singular chemotherapy.

3. Conclusions

The fusogenic porous silicon nanoparticles (FNPs) demonstrated three materials aspects that are crucial for effective siRNA-mediated gene therapy. First, peptide targeting moieties enabled the FNPs to selectively home to and transfect the desired cell target; in this work we focused on cancer cell types (tumor associated macrophages and tumor cells) and we previously demonstrated that another peptide can home FNPs to and transfect macrophages[8], establishing this as a relatively general approach. Second, effective delivery of the gene payload to the interior of the cell was afforded by the fusogenic lipid coating, which allowed the nanoparticles to avoid the endocytosis pathway. The fusogenic nature of these lipid coatings enabled a third crucial aspect: the specific, triggered release of the nucleic acid payload. The lipid stabilized the calcium silicate nanoparticle chemistry until cellular fusion had stripped the lipids, at which point rapid dissolution of the porous silicon nanoparticle ensued such that free siRNA was released into the cytosol. A strong gene silencing effect was observed both *in vitro* (> 90%) and *in vivo* (> 80%), which compares favorably to the average of 57.4 ± 21% *in vitro* (N=54) and 55.0 ± 17% *in vivo* (N=13) for gene therapy found across the literature[40].

A primary goal of this study was to understand the mechanism by which the FNPs operate. We showed that the lipid composition has a direct influence on its behavior, and that a combination of properties (fluidity, cationic charge, and PEGylation) allows for plasma membrane fusion and endocytic bypass. Biological inhibitor studies showed that FNPs enter cells independently of typical endocytic pathways and intracellular vesicle traffic routes. However, vesicle fusion and certain exocytosis pathways were found to influence the fate of FNPs. The exact mechanism by which the fusogenic coating interacts with these pathways remains to be studied, as the extent of existing knowledge regarding these cellular pathways is limited.

The general nature of this approach was established and exemplified using two therapeutic formulations: (1) gene therapy (C-FNPs) to sensitize cancer cells to chemotherapy; and (2) immunotherapy (T-FNPs) to polarize macrophages toward the tumorigenic M2 phenotype. Each used a different targeting peptide for cell specificity and a different siRNA to program the desired genetic outcome. Combining homing specificity with high *in vivo* gene knockdown capabilities, the system showed a strong synergy in combination with a first-line

chemotherapeutic, cisplatin, that showed significant reduction (and in some cases, complete elimination) of tumors in an ovarian cancer mouse model.

4. Experimental Section

Materials:

Highly boron-doped p-type silicon wafers (~1 mΩ-cm resistivity, polished on the (100) face) were obtained from Virginia Semiconductor, Inc or Siltronix, Inc. Hydrofluoric acid (48% aqueous, ACS grade) was obtained from Fisher Scientific. Anhydrous calcium chloride was obtained from Spectrum Chemicals (Gardena, CA). Deionized (18 mΩ) water was used for all aqueous dilutions. For lipids, 1,2-dimyristoyl-sn-glycero-3-phosphocholine (DMPC), 1,2-distearoyl-sn-glycero-3-phosphoethanolamine-N-[methoxy(polyethylene glycol)-2000], (DSPE-mPEG), 1,2-distearoyl-sn-glycero-3-phosphoethanolamine-N-[maleimide(polyethylene glycol)-2000] (DSPE-PEG-maleimide), and 1,2-dioleoyl-3-trimethylammonium-propane (DOTAP) were purchased from Avanti Polar Lipids (Alabaster, AL) and stored at -4°C. The fluorescent lipophilic dyes 1,1'-dioctadecyl-3,3,3',3'-tetramethylindocarbocyanine perchlorate (DiI) and 3,3'-dioctadecyloxacarbocyanine perchlorate (DiO) were obtained from Life Technologies, and Lipofectamine® 2000 transfection reagent was obtained from Thermo Fisher Scientific. Custom siRNA against luciferase (siLuc) was purchased from Dharmacon (Lafayette, CO), and primers were purchased from IDT DNA (San Diego, CA). Silencer ® Pre-designed siRNA encoding for PI3Kγ (siPI3Kγ; sequence: GGACCACGAGAGUGUGUUCtt) was purchased from Life Technologies, and siGENOME Human REV3L siRNA (siREV3L; sequence: CUGCAGAGAGAAUAACCCUGAdTdT) was purchased from Dharmacon. The siRNAs against *Cav1* (10297), *Cltc* (107565), *Rac1* (120601), *Rab11* (122729), *Rab5a* (120371), *Stx6* (121571), *T-snare* (127901), *Rab27b* (120374) were purchased from Thermo Fisher Scientific (Waltham, MA). Targeting peptides (LyP-1 and iRGD) were custom synthesized by CTC Scientific (Sunnyvale, CA). For *in vitro* studies, J774a.1 cells were purchased from ATCC (Manassas, VA) within 6 months prior to all experiments. DMEM cell media was purchased from GE Healthcare Life Sciences (HyClone, Pittsburg, PA), with supplemental fetal bovine serum (HyClone, Pittsburg, PA) and penicillin/streptomycin (HyClone, Pittsburg, PA). The Cell counting kit-8 (CCK-8) was purchased from Dojindo Molecular Technologies, Inc. (Rockville, MD). Corning Matrigel Membrane Matrix was purchased from Fisher Scientific. Six week-old female athymic nu/nu mice were purchased from Envigo (Placentia, CA).

Preparation of porous silicon nanoparticles:

Porous silicon (pSi) samples were prepared as previously established by electrochemical etching of silicon wafers by applying a square waveform current density of 50 mA/cm^2 for 0.6s and high current density of 400 mA/cm^2 for 0.36s, repeated for 200 cycles (CAUTION: HF is highly toxic and proper care should be exerted to avoid contact with skin or lungs) [8, 12]. After detaching the porous layer, the porous silicon nanoparticles (pSiNPs) were generated by ultrasonic fracture (50T ultrasonic bath, VWR International) of porous silicon (0.8 mg) in RNAse-free water (2 mL) for 12h. The siRNA payloads were loaded into pSiNPs by calcium silicate sealing, as described previously[8, 11]. The oligonucleotide

payload was hydrated in RNAse-free water to generate a 20 μM solution. 150 μL of siRNA was pipetted gently into a solution prepared from 150 μL of the pSiNP dispersion and 700 μL of 2M calcium chloride and the mixture was subjected to ultrasonication for 15 min. We used siREV3L (GAG AGU ACC UCC AGA UUU A), siPI3Kg (GGA CCA CGA GAG UGU GUU Ctt) and siLuc (CUU ACG CUG AGU ACU UCG A) for all relevant experiments.

Fusogenic coating:

Fusogenic (FNP) and non-fusogenic (NNP) coatings were prepared using estbalished methods[8, 12]. Briefly, lipid films of DMPC, DSPE-PEG, and DOTAP at molar ratios of 76.2:3.8:20 (FNP) and 96.2:3.8:20 (NNP) were prepared by evaporating the organic solvent, and we added 20 μL of DiI or DiO (1.25 mg/ml in 100% ethanol) for lipophilic dye incorporation. The films were then hydrated and extruded with the siRNA-loaded pSiNPs. Next, 100 μL of 1 mg/mL of targeting peptides (iRGD and LyP-1) were added to the extruded product to conjugate the peptides to maleimide-terminated DSPE-PEG overnight at 4°C. Particles were washed three times at each step by centrifugation in a Microcon-30kDa Centrifugal Filter Unit (EMD Millipore) by spinning at 5,000g at 25°C. A video protocol of FNP synthesis available from [12].

The alternative formulations to the fusogenic nanoparticles were synthesized in the exact same manner as the fusogenic nanoparticles, albeit with different lipid compositions in the coating. In the DSPC particle, the composition was DSPC:DOTAP:DSPE-PEG at molar ratio of 76.2:3.8:20; in the DLPC particle, the composition was DLPC:DOTAP:DSPE-PEG at molar ratio of 76.2:3.8:20; in the DOTMA particle, the composition was DMPC:DOTMA:DSPE-PEG at molar ratio of 76.2:3.8:20; and in the non-PEGylated particle, the composition was DMPC:DOTAP at molar ratio of 76.2:20. Again, we added 26.3 μg of DiI (1.25 mg/mL in 100% ethanol) to incorporate lipophilic DiI into the films. All lipids were mixed at concentration of 10 mg/mL and the organic solvent was evaporated. The films were then hydrated with a solution of the payload-containing pSiNPs and prepared by the same abovementioned film hydration/extrusion method.

Nanoparticle size and zeta-potential were measured by dynamic light scattering (DLS, Zetasizer ZS90, Malvern Instruments), and structural morphology was visualized with a JEOL 1200 EX II TEM or FEI Tecnai Spirit G2 BioTWIN TEM, as indicated in figure captions. Samples were prepared by dropping 5 μL of the sample on the TEM grid, drying off excess solvent after 1 min, and dropping 5 μL of uranyl acetate for negative staining. The siRNA loading was quantified using a NanoDrop 2000 spectrophotometer (Thermo Fisher Scientific, ND-2000) to measure the total siRNA released, and it was purified from the formulations after suspending the particles in ethanol for lipid dissassembly and dispersion (or lysing the lipid coating using 0.1% Triton-X 100), isolating the core particles into pellets by centrifugation at 13,000g, and dissolving all pSiNPs by resuspension of the pellet in PBS and shaking on a vortexer overnight.

In vitro siRNA release:

Porous silicon core nanoparticles without lipid coating (pSiNPs), FNPs, and NNPs containing 11.9 μg of siPI3Kγ were incubated at 37°C in 400 μL of PBS. The particles were removed from incubation and centrifuged in a Microcon-30kDa Centrifugal Filter Unit (EMD Millipore) by spinning at 5,000g at 25°C for 30 min. The released siRNA concentration was quantified by measuring the supernatant with a NanoDrop 2000 spectrophotometer. Upon removal of the supernatant, 400 μL of fresh PBS was used to resuspend the particle pellets. The particles were kept in the incubator until each time point when the above measurement steps were repeated. The total siRNA release was summed up and averaged over six independent trials.

Cell culture:

CAOV-3 human ovarian adenocarcinoma and J774a.1 murine macrophage lines were cultured in DMEM supplemented with 10% FBS and 1% penicillin/streptomycin, and were incubated at 37°C in 5% CO_2.

Confocal microscopy:

All confocal microscopy images are representative of at least three independent trials and of at least 1×10^6 cells per slide. Fusion of DiI-loaded or siRNA-loaded particles was observed by seeding 0.3×10^6 cells on top of 22 mm round coverslips (BD Biocoat Collagen Coverslip, 22 mm) in a 6-well plate, growing to 80% confluence, and treating the cells with 10 μL of nanoparticles. The particle-treated CAOV-3 cells were incubated at 37℃ in 5% CO_2 for 15 min, whereas the particle-treated J774a.1 cells were incubated for 5 min. After incubation, the cells were washed in PBS three times to remove any particles that were not taken up. The cells were fixed in 1% paraformaldehyde (PFA, Santa Cruz Biotechnology) for 10 min at 4°C, then washed with PBS three times. The coverslips were mounted on glass slides with ProLong® Diamond Antifade Mountant with DAPI (Life Technologies), dried and kept in the dark until examined by confocal microscopy (Zeiss LSM 710 NLO).

For studies involving lysosome staining, 0.3×10^6 cells were seeded on 35 mm petri dishes, and grown to 80% confluence. The cells were pre-stained with LysoTracker Green (Thermo Fisher Scientific) for 1h at 37°C in 5% CO_2 according to manufacturer's instructions. The cells were then washed with PBS three times, and then treated with 10 μL of DiI-loaded particles for 15 min (CAOV-3) or 5 min (J774a.1) at 37℃ in 5% CO_2. The cells were washed with PBS three times to remove any particles that were not taken up, and the wells were filled with 1 mL of PBS and immediately subjected to live-cell imaging by confocal microscopy (Zeiss LSM 710 NLO). Pearson's correlation coefficient (PCC) for co-localization was calculated using the Coloc2 plugin from the ImageJ software package (NIH). At least ten representative images were analyzed to obtain the average coefficient.

For imaging porous silicon core nanoparticles or Cy3-tagged siIRF5 as a model siRNA, 0.3 $\times 10^6$ cells were seeded on 35 mm petri dishes, and grown to 80% confluence. The cells were treated with 10 μL of DiO-loaded fusogenic or non-fusogenic particles with either Cy3-tagged or non-tagged siIRF5-loaded pSiNP cores for 15 min at 37℃ in 5% CO_2. The cells were washed with PBS three times to remove any particles that were not taken up, then

fixed in 1% paraformaldehyde (PFA, Santa Cruz Biotechnology) for 10 min at 4°C, then washed with PBS three times. The coverslips were mounted on glass slides with ProLong® Diamond Antifade Mountant with DAPI (Life Technologies), dried and kept in the dark until examined by confocal microscopy (Zeiss LSM 710 NLO). For Cy3 imaging, λ_{ex} = 550 nm and λ_{em} = 580–630 nm band-pass was used, and for pSiNP imaging, λ_{ex} = 370 nm and λ_{em} = 650 nm long-pass was used.

In vitro biomarker studies:

For the mechanistic studies involving cellular uptake and intracellular trafficking of the DiI-stained lipids on the fusogenic nanoparticles, we seeded 6-well plates with 0.3×10^6 CAOV-3 cells on top of coverslips. At 70% confluence, we transfected the cells with 100 pmol of siRNAs (against Cav1, *Cltc, Rac1, Rab11, Rab5a, Stx6, T-snare, or Rab27b*) and 5 μL of Lipofectamine 2000 transfection agent per well, as per the manufacturer's instructions. The cells were incubated with the transfectant for 4h at 37°C in 5% CO_2, then washed three times with PBS. The wells were replaced with 2 mL of fresh DMEM supplemented with 10% FBS and 1% penicillin/streptomycin, and further incubated for 48h. The cells were then treated with 10 μL of nanoparticles and incubated at 37°C in 5% CO_2 for 15 min, then washed with PBS three times, then fixed, dried, and mounted with DAPI as described above. For experiments with lysosome staining, the cells were stained with LysoTracker Green for 1h at 37°C in 5% CO_2 according to the manufacturer's instructions, prior to particle treatment and live-cell imaging by confocal microscopy.

To determine the exocytosis pathway for fusogenic nanoparticles, we used a transwell culture system. We seeded 0.1×10^6 CAOV-3 cells in the top well, and placed them on top of an empty 6-well plate, and 0.3×10^6 CAOV-3 cells on coverslips were seeded in another 6-well plate to serve as the lower well post-inhibition. At 60% confluence, we treated the cells in the top wells with 10 μM of Bisindolymaleimide I (BIM I), or 10 μM of GW4869 for 24h at 37°C in 5% CO_2, or 100 pmol of siRNA against *Rab27b* with 5 μL of Lipofectamine 2000 for 4h at 37°C in 5% CO_2, then washed with PBS three times to be further incubated for 48h. Post-inhibition of exocytosis, the cells were treated with particles (10 μL) for 30 min at 37°C in 5% CO_2, then washed with PBS three times. The top wells were then transferred to the lower wells in the 6-well plate with CAOV-3 cultured on the coverslips with fresh DMEM supplemented with 10% FBS and 1% penicillin/streptomycin, and further incubated for 48h. The lower well cells were washed with PBS three times, fixed and mounted with DAPI and analyzed by confocal microscopy as described above.

For all particle uptake quantifications, we used Image J software to quantify the brightness and area taken up by the DiI signals for each condition. The values were averaged over 12 measurements per 10 representative images taken per well. Statistics were performed using Student's paired t-test with α-level of 0.05.

In vitro siRNA silencing:

In vitro knockdown efficiencies of the nanoformulations were quantified using two-step quantitative real-time reverse transcription polymerase chain reaction (qRT-PCR, Roche LightCycler 96).

For the dose-response of the siRNA against *rev3l* (siREV3L), we seeded 0.25×10^6 CAOV-3 cells per well in a 24 well-plate. At 50% confluence, we treated the cells at 0, 0.5, 2.5, 5, 12.5, 25, 50, and 100 nM siREV3L doses of Lipofectamine, fusogenic nanoparticles (FNPs) and non-fusogenic nanoparticle (NNPs). While the Lipofectamine formulations were incubated for 4h, the FNPs and NNPs were treated for 1h, then washed with PBS three times. The wells were replaced with fresh DMEM supplemented with 10% FBS and 1% penicillin/streptomycin, and further incubated for 48h. Post-incubation, RNA purification, cDNA synthesis, and RT-PCR analysis were conducted as previously published[8]. cDNA was mixed with REV3L primers, or the control HPRT primers (REV3L forward: AGGACTCGAAGTCACCTATGC; REV3L reverse: AGAGGTAACCCCAGGAATGC; HPRT forward: GTCAACGGGGGACATAAAAG; HPRT reverse: CAACAATCAAGACATT-CTTTCCA) and iQ SYBR Green Supermix according to the manufacturer's instructions. The quantification was performed at n=8 and in RNAse- and DNAse-free laminar flow hood dedicated to RNA work.

For quantification of *in vitro* knockdown efficiency of siRNA against PI3Kγ (siPI3Kγ), we seeded 0.25×10^6 J774a.1 cells per well in a 24-well plate. At 50% confluence, we treated the cells at 50 and 100 nM siPI3Kγ doses of Lipofectamine, fusogenic nanoparticles (FNPs) and non-fusogenic nanoparticle (NNPs). The transfection and qRT-PCR protocol were identical to the dose-response study described above, with primers for PI3Kγ (PI3Kγ forward: GGCTCAAAGAAAAATCCCCTA; PI3Kγ reverse: AGCCTGCACAGGAATAAACAA).

Cell viability assay:

Cell viability was determined by seeding 96 well-plates with 0.01×10^6 CAOV-3 or J774a.1 cells per well. At 50% confluence, we treated each well at the 50 nM siRNA dose of Lipofectamine (0.25 μL per well), FNPs, FNPs loaded with siLuc, NFPs, or PBS as the control group. The formulations were incubated for 1h (4h for Lipofectamine group) at 37°C in 5% CO_2, then washed with PBS three times and further incubated for 48h. The CCK-8 cytotoxicity assay was performed according to manufacturer's instructions. In brief, the CAOV-3 cells were treated with 10 μL of the CCK-8 solution per well, and incubated for 2h. The absorbance at 450 nm was measured using the UV-Vis microplate reader for quantification of cell viability. The cell viability was averaged over 10 wells per group, and normalized to the viability of the PBS control treatment group. Single-way ANOVA was used with α-level of 0.01 to determine significant differences between the formulations.

For the *in vitro* CDDP-siREV3L interaction study, we seeded a 96 well-plate with 0.01×10^6 CAOV-3 cells per well. At 50% confluence, we treated each well at the 50 nM siRNA dose of Lipofectamine (0.25 μL per well), FNPs, FNPs loaded with siLuc, NFPs, or PBS as the control group. The formulations were incubated for 1h (4h for Lipofectamine group) at 37°C in 5% CO_2, then washed with PBS three times and further incubated for 48h. Post-transfection, the media was removed, and the cells were treated with increasing doses of CDDP (0, 0.01, 0.1, 1, 10, 25, 50, and 100 μg/mL in PBS) per treatment group. The cells were incubated with CDDP for 24h at 37°C in 5% CO_2, then washed with PBS three times. The CCK-8 cytotoxicity was assay was used as described above to quantify the cell viability

of each treatment group at the treated CDDP doses. Cell viability for the 0 μg/mL CDDP treatment in the PBS control group was used as the normalization control, and each result was averaged over 10 independent trials. The IC_{50} of each treatment was extrapolated from the results.

Mouse Model:

Ovarian cancer xenografts were established in athymic nude mice (6–8 week old, female) by subcutaneously injecting 5×10^6 CAOV-3 cells in PBS and Matrigel media mixed at 1:1 ratio. For the peritoneal carcinomatosis model, we performed intraperitoneal injection of 3×10^6 CAOV-3 cells in PBS. Only female mice were used in this study, as ovarian cancer is only relevant for the female population. All animals for the *in vivo* studies were handled, anesthetized, and euthanized according to the Institutional Animal Care and Use Committee (IACUC) guidelines. All animal experiments were performed independent of each other with different cohorts of mice.

Statistics:

All statistical analyses were performed using single way ANOVA and post hoc comparisons using Tukey's HSD test at $p < 0.05$, unless otherwise stated. Power analysis was performed to estimate the total mouse sample size required for the tumor growth and survival studies using the GPower 3.1 software. The analysis was performed using *a priori*, ANOVA: repeated measures, between factors, as the study looks at tumor growth by each therapeutic formulation over time. Based on a published study[8] (N=32), where the fusogenic nanoparticles were intravenously injected for siRNA knockdown in Balb/C mice with bacterial infection, the effect size (ES) was calculated to be 11.5, thus set to 'large' (0.40) in the software's parameter settings. With α error probability of 0.05 and Power of 0.80, 5 test groups, 15 measurements (for tumor size), and correlation of 0.3, we determined that a sample size of 35 mice was adequate for the experiments investigating the therapeutic efficacy of the formulations.

Biosafety of fusogenic nanoparticles:

For *in vivo* biosafety evaluation, healthy athymic nu/nu mice were intravenously injected with T-FNP or C-FNP at 100 μmol/kg lipid, corresponding to 62.5 μg/kg siRNA, and 641 μg/kg pSi in 100 μL PBS. After 24h circulation, the mice were sacrificed under deep isofluorane anesthesia (no response to toe pinch) by cardiac perfusion, and brain, heart, lungs, liver, kidneys, and spleen were harvested. Organs were fixed immediately in 4% PFA, and sent to the University of California, San Diego (UCSD)'s histology core to be paraffinized and sectioned for hematoxylin and eosin (H&E) staining. The stained slides were histopathologically evaluated by Dr. Kent Osborn (Associate Director, Animal Care Program, UCSD).

Nanoparticle biodistribution:

After establishment of the tumor mouse model, the tumor nodules were allowed to grow for 3 weeks. The mice were then IP injected with PBS, FNP, T-FNP, or C-FNP formulations loaded with DiI at 100 μmol/kg lipid corresponding to 641 μg/kg pSi in 100 μL PBS. After

1h or 24h, the mice were sacrificed following a standard perfusion protocol using 50 mL of 4% PFA, and the major organs (heart, lungs, liver, spleen, kidneys) and the tumor nodules were harvested and immediately fixed in 4% PFA. The organs were imaged for DiI fluorescence using an IVIS 200 imaging system (Perkin-Elmer) with 0.1s exposure time and excitation/emission filters set at 500/520 nm. The DiI accumulation was quantified based on five mouse images per formulation and time group using Image J analysis. The quantified uptake was statistically analyzed using one-way ANOVA with Tukey's post hoc analysis. The same experiment was performed with xenograft mice by intravenous injection of the particles.

Flow Cytometry:

After establishment of the mouse tumor model, the tumor nodules were allowed to grow for 3 weeks. The mice were then IP injected with PBS, FNP, T-FNP, C-FNP, or a 50:50 cocktail mix of T-FNP and C-FNP formulations loaded with DiI (peptides were tagged with FAM) at 100 μmol/kg lipid corresponding to 641 μg/kg pSi in 100 μL PBS. After 24h, the mice were sacrificed for macrophage and tumor collection. First, we performed intraperitoneal lavage using 3–5 mL of 4% PFA in a 20G syringe. After aspirating cells from the peritoneal cavity, we opened up the cavity for tumor nodule collection. We then homogenized the tumor nodules for further cell separation. Both the lavage and tumor homogenates were treated with Dead Cell Removal MicroBeads (Miltenyi Biotec) for magnetic separation on an LS column according to the manufacturer's instructions. The collected cells were then treated with Anti-F4/80 microbeads (Miltenyi Biotec) for magnetic separation on an LS column according to the manufacturer's instructions to collect only the macrophages. The macrophages from the lavage and tumor homogenates, as well as the tumor cells were run through a LSRFortessa flow cytometer (BD Biosciences) to analyze the number of cells containing either the particles' DiI signals (ex: 561 nm/50 mW; em: 582/15 nm) or the peptides' FAM signals (ex: 488 nm/50 mW; em: 510/25 nm). The results were analyzed and presented using FlowJo v10 software (FlowJo, LLC).

In vivo siRNA silencing:

After establishment of the mouse tumor model, the tumor nodules were allowed to grow for 3 weeks. The mice were then IP injected with PBS, T-FNP or C-FNP at 100 μmol/kg lipid, corresponding to 62.5 μg/kg siRNA, and 641 μg/kg pSi in 100 μL PBS. After 48h, the mice were sacrificed for macrophage and tumor collection. First, we performed intraperitoneal lavage using 3–5 mL of 4% PFA in a 20G syringe. After aspirating cells from the peritoneal cavity, we opened up the cavity for tumor nodule collection. We then homogenized the tumor nodules for further cell separation. Both the lavage and tumor homogenates were treated with Dead Cell Removal MicroBeads (Miltenyi Biotec) for magnetic separation on an LS column according to the manufacturer's instructions. The collected cells were then treated with Anti-F4/80 microbeads (Miltenyi Biotec) for magnetic separation on an LS column according to the manufacturer's instructions to collect only the macrophages. The macrophages from the lavage and tumor homogenates, as well as the tumor cells were collected by centrifugation post-magnetic separation by centrifugation at 300g for 5 min at 4°C.

The degree of knockdown of *pi3kγ* in the macrophages and of *rev3l* in the tumor cells was quantified using two-step qRT-PCR (Roche LightCycler 96). The cells were lysed for RNA purification using QIAshredder and RNeasy Mini Kit (Qiagen, Valencia, Ca). cDNA was transcribed from the purified RNA using the BIORAD iScript cDNA Synthesis Kit and heat-treated in the Eppendorf Vapo.protect Mastercycler thermal cycler. cDNA was mixed with PI3Kγ primers for macrophages and REV3L primers for the tumor cells, with HPRT primers as control for both cells (PI3Kγ forward: GGCTCAAAGAAAAATCCCCTA; PI3Kγ reverse: AGCCTGCACAGGAATAAACAA; REV3L forward: TGAGTTCAAATTTGGCTGTACCT; REV3L reverse: TCTAGTCTTCAAAATTTCTTCAAGCA; HPRT forward: GTCAACGGGGGACATAAAAG; HPRT reverse: CAACAATCAAGACATTCTTTCCA) and iQ SYBR Green Supermix according to the manufacturer's instructions. qRT-PCR analysis was performed in BIORAD 96-well white Multiplate PCR Plates using the Roche LightCycler 96. The quantification was performed at n=6 and in a RNAse- and DNAse-free laminar flow hood dedicated to RNA work. Relative knockdown was statistically evaluated using one-way ANOVA with Tukey's HSD post-hoc analysis.

In vivo therapeutic efficacy of fusogenic nanoparticles:

After establishment of the mouse tumor model, the tumor nodules were allowed to grow for 1 week. The mice were then IP injected with PBS, CDDP (2 mg/kg), 1:1 cocktail of CDDP (2 mg/kg) with T-FNP, 1:1 cocktail of CDDP (2 mg/kg) with C-FNP, or a 1:1:1 cocktail of CDDP (2 mg/kg) with T-FNP and C-FNP at 70.2 μmol/kg lipid, corresponding to 36.1 μg/kg siRNA, and 451 μg/kg pSi in 100 μL PBS. The mice were IP injected with 2 mg/kg of CDDP every 3 days, and the T- and C-FNP formulations every 7 days. After 30 days, the mice were sacrificed and opened for tumor nodule collection. The number of tumor nodules were counted and the size of tumor nodules were measured on the longest dimension using a caliper. The results were analyzed by one-way ANOVA with Tukey's HSD post-hoc analysis.

Supplementary Material

Refer to Web version on PubMed Central for supplementary material.

Acknowledgements

have been reviewed and approved by the University of California, San Diego in accordance with its conflict of interest policies. E.R. is a founder, officer, and shareholder of DrugCendR Inc. which holds a license to the iRGD peptide.

References

[1]. Sun J, Wei Q, Zhou Y, Wang J, Liu Q, Xu H, BMC Syst Biol 2017, 11, 87. [PubMed: 28984210]

[2]. Wood H, Nat Rev Neurol 2018, 14, 570.

[3]. Gilleron J, Querbes W, Zeigerer A, Borodovsky A, Marsico G, Schubert U, Manygoats K, Seifert S, Andree C, Stoter M, Epstein-Barash H, Zhang L, Koteliansky V, Fitzgerald K, Fava E, Bickle M, Kalaidzidis Y, Akinc A, Maier M, Zerial M, Nature biotechnology 2013, 31, 638;Sahay G, Querbes W, Alabi C, Eltoukhy A, Sarkar S, Zurenko C, Karagiannis E, Love K, Chen D, Zoncu R, Buganim Y, Schroeder A, Langer R, Anderson DG, Nature biotechnology 2013, 31, 653.

[4]. Wang Y, Huang L, Nat Biotechnol 2013, 31, 611. [PubMed: 23839146]

[5]. Lewis JG, Lin KY, Kothavale A, Flanagan WM, Matteucci MD, DePrince RB, Mook RA, Hendren RW, Wagner RW, Proc. Natl. Acad. Sci. U. S. A 1996, 93, 3176. [PubMed: 8622909]

[6]. Torchilin VP, Nat Rev Drug Discov 2005, 4, 145. [PubMed: 15688077]

[7]. Ozpolat B, Sood AK, Lopez-Berestein G, Adv Drug Deliv Rev 2014, 66, 110. [PubMed: 24384374]

[8]. Kim B, Pang HB, Kang J, Park JH, Ruoslahti E, Sailor MJ, Nat Commun 2018, 9, 1969. [PubMed: 29773788]

[9]. Russell LM, Hultz M, Searson PC, J Control Release 2018, 269, 171. [PubMed: 29122661]

[10]. Tanaka T, Mangala LS, Vivas-Mejia PE, Nieves-Alicea R, Mann AP, Mora E, Han HD, Shahzad MM, Liu X, Bhavane R, Gu J, Fakhoury JR, Chiappini C, Lu C, Matsuo K, Godin B, Stone RL, Nick AM, Lopez-Berestein G, Sood AK, Ferrari M, Cancer Res 2010, 70, 3687. [PubMed: 20430760]

[11]. Kang J, Joo J, Kwon EJ, Skalak M, Hussain S, She ZG, Ruoslahti E, Bhatia SN, Sailor MJ, Adv Mater 2016, 28, 7962. [PubMed: 27383373]

[12]. Kim B, Sailor MJ, JoVE 2019, e59440.

[13]. Choi E, Lee J, Kwon IC, Kim S, Biomaterials 2019.

[14]. Hasanzadeh Kafshgari M, Delalat B, Tong WY, Harding F, Kaasalainen M, Salonen J, Voelcker N, Oligonucleotide delivery by chitosan-functionalized porous silicon nanoparticles, Vol. 8, 2015;Ashley CE, Carnes EC, Epler KE, Padilla DP, Phillips GK, Castillo RE, Wilkinson DC, Wilkinson BS, Burgard CA, Kalinich RM, Townson JL, Chackerian B, Willman CL, Peabody DS, Wharton W, Brinker CJ, ACS Nano 2012, 6, 2174; [PubMed: 22309035] Basha G, Novobrantseva TI, Rosin N, Tam YY, Hafez IM, Wong MK, Sugo T, Ruda VM, Qin J, Klebanov B, Ciufolini M, Akinc A, Tam YK, Hope MJ, Cullis PR, Mol Ther 2011, 19, 2186; [PubMed: 21971424] Meng HA, Liong M, Xia TA, Li ZX, Ji ZX, Zink JI, Nel AE, ACS Nano 2010, 4, 4539; [PubMed: 20731437] Woodrow KA, Cu Y, Booth CJ, Saucier-Sawyer JK, Wood MJ, Saltzman WM, Nat Mater 2009, 8, 526; [PubMed: 19404239] Oh YK, Park TG, Adv Drug Deliv Rev 2009, 61, 850; [PubMed: 19422869] Howard KA, Adv Drug Deliv Rev 2009, 61, 710; [PubMed: 19356738] Zhang S, Zhao B, Jiang H, Wang B, Ma B, J Control Release 2007, 123, 1. [PubMed: 17716771]

[15]. Lee J, Kim J, Jeong M, Lee H, Goh U, Kim H, Kim B, Park JH, Nano Lett 2015, 15, 2938; [PubMed: 25806671] Kim J, Santos OA, Park JH, J Control Release 2014, 191, 98. [PubMed: 24892975]

[16]. Balazs DA, Godbey W, Journal of Drug Delivery 2011, 2011.

[17]. Lentz BR, Chem Phys Lipids 1994, 73, 91; [PubMed: 8001186] Dennison SM, Bowen ME, Brunger AT, Lentz BR, Biophys J 2006, 90, 1661. [PubMed: 16339880]

[18]. Sun J, Jakobsson E, Wang Y, Brinker C, Life 2015, 5, 214; [PubMed: 25607812] Liu J, Stace-Naughton A, Jiang X, Brinker CJ, Journal of the American Chemical Society 2009, 131, 1354. [PubMed: 19173660]

[19]. Wang J, Kumeria T, Bezem MT, Wang J, Sailor MJ, ACS Appl Mater Interfaces 2018, 10, 3200. [PubMed: 29278488]

[20]. Park JH, Gu L, von Maltzahn G, Ruoslahti E, Bhatia SN, Sailor MJ, Nat Mater 2009, 8, 331. [PubMed: 19234444]

[21]. Kube S, Hersch N, Naumovska E, Gensch T, Hendriks J, Franzen A, Landvogt L, Siebrasse J-P, Kubitscheck U, Hoffmann B, Merkel R, Csiszár A, Langmuir 2017, 33, 1051; [PubMed: 28059515] Ozpolat B, Sood AK, Lopez-Berestein G, Adv. Drug Deliv. Rev 2014, 66, 110; [PubMed: 24384374] Kraft JC, Freeling JP, Wang Z, Ho RJY, J. Pharm. Sci 2014, 103, 29; [PubMed: 24338748] Allen TM, Cullis PR, Adv. Drug Deliv. Rev 2013, 65, 36. [PubMed: 23036225]

[22]. Jiang W, Lionberger RA, Yu LX, Bioanalysis 2011, 3, 333; [PubMed: 21320053] Russell LM, Hultz M, Searson PC, Journal of Controlled Release 2018, 269, 171; [PubMed: 29122661] Hasan W, Chu K, Gullapalli A, Dunn SS, Enlow EM, Luft JC, Tian SM, Napier ME, Pohlhaus PD, Rolland JP, DeSimone JM, Nano Lett 2012, 12, 287. [PubMed: 22165988]

[23]. Park J-H, Gu L, Maltzahn G. v., Ruoslahti E, Bhatia SN, Sailor MJ, Nature Mater 2009, 8, 331. [PubMed: 19234444]

[24]. Jin Y, Kim D, Roh H, Kim S, Hussain S, Kang J, Pack C-G, Kim JK, Myung S-J, Ruoslahti E, Sailor MJ, Kim SC, Joo J, Adv. Mater 2018, 30, 1802878.

[25]. Gore ME, Fryatt I, Wiltshaw E, Dawson T, Gynecol Oncol 1990, 36, 207; [PubMed: 2404837] Matsuo K, Lin YG, Roman LD, Sood AK, Expert Opin Investig Drugs 2010, 19, 1339.

[26]. Morgan RD, Clamp AR, Evans DGR, Edmondson RJ, Jayson GC, Cancer Chemother Pharmacol 2018, 81, 647. [PubMed: 29464354]

[27]. Siddik ZH, Oncogene 2003, 22, 7265. [PubMed: 14576837]

[28]. da Cunha Colombo Bonadio RR, Fogace RN, Miranda VC, Diz M, Clinics (Sao Paulo) 2018, 73, e450s. [PubMed: 30133561]

[29]. Doles J, Oliver TG, Cameron ER, Hsu G, Jacks T, Walker GC, Hemann MT, Proc Natl Acad Sci U S A 2010, 107, 20786; [PubMed: 21068376] Jiang HG, Chen P, Su JY, Wu M, Qian H, Wang Y, Li J, J Cell Physiol 2017;Dai CH, Chen P, Li J, Lan T, Chen YC, Qian H, Chen K, Li MY, Oncotarget 2016;Wu F, Lin X, Okuda T, Howell SB, Cancer Res 2004, 64, 8029. [PubMed: 15520212]

[30]. Sugahara KN, Scodeller P, Braun GB, de Mendoza TH, Yamazaki CM, Kluger MD, Kitayama J, Alvarez E, Howell SB, Teesalu T, Ruoslahti E, Lowy AM, J Control Release 2015, 212, 59. [PubMed: 26071630]

[31]. Coussens LM, Zitvogel L, Palucka AK, Science 2013, 339, 286; [PubMed: 23329041] Germano G, Frapolli R, Belgiovine C, Anselmo A, Pesce S, Liguori M, Erba E, Uboldi S, Zucchetti M, Pasqualini F, Nebuloni M, van Rooijen N, Mortarini R, Beltrame L, Marchini S, Fuso Nerini I, Sanfilippo R, Casali PG, Pilotti S, Galmarini CM, Anichini A, Mantovani A, D'Incalci M, Allavena P, Cancer Cell 2013, 23, 249; [PubMed: 23410977] Mantovani A, Bottazzi B, Colotta F, Sozzani S, Ruco L, Immunol Today 1992, 13, 265; [PubMed: 1388654] Noy R, Pollard JW, Immunity 2014, 41, 49; [PubMed: 25035953] Ries CH, Cannarile MA, Hoves S, Benz J, Wartha K, Runza V, Rey-Giraud F, Pradel LP, Feuerhake F, Klaman I, Jones T, Jucknischke U, Scheiblich S, Kaluza K, Gorr IH, Walz A, Abiraj K, Cassier PA, Sica A, Gomez-Roca C, de Visser KE, Italiano A, Le Tourneau C, Delord JP, Levitsky H, Blay JY, Ruttinger D, Cancer Cell 2014, 25, 846; [PubMed: 24898549] Williams CB, Yeh ES, Soloff AC, NPJ Breast Cancer 2016, 2;Mantovani A, Marchesi F, Malesci A, Laghi L, Allavena P, Nature Reviews Clinical Oncology 2017, 14, 399.

[32]. Foubert P, Kaneda MM, Varner JA, Cancer Immunol Res 2017, 5, 957; [PubMed: 28963139] Kaneda MM, Messer KS, Ralainirina N, Li H, Leem CJ, Gorjestani S, Woo G, Nguyen AV, Figueiredo CC, Foubert P, Schmid MC, Pink M, Winkler DG, Rausch M, Palombella VJ, Kutok J, McGovern K, Frazer KA, Wu X, Karin M, Sasik R, Cohen EE, Varner JA, Nature 2016, 539, 437; [PubMed: 27642729] Schmid MC, Avraamides CJ, Dippold HC, Franco I, Foubert P, Ellies LG, Acevedo LM, Manglicmot JR, Song X, Wrasidlo W, Blair SL, Ginsberg MH, Cheresh DA, Hirsch E, Field SJ, Varner JA, Cancer Cell 2011, 19, 715; [PubMed: 21665146] De Henau O, Rausch M, Winkler D, Campesato LF, Liu C, Cymerman DH, Budhu S, Ghosh A, Pink M, Tchaicha J, Douglas M, Tibbitts T, Sharma S, Proctor J, Kosmider N, White K, Stern H, Soglia J, Adams J, Palombella VJ, McGovern K, Kutok JL, Wolchok JD, Merghoub T, Nature 2016, 539, 443. [PubMed: 27828943]

[33]. Uchida M, Kosuge H, Terashima M, Willits DA, Liepold LO, Young MJ, McConnell MV, Douglas T, ACS Nano 2011, 5, 2493; [PubMed: 21391720] Scodeller P, Simon-Gracia L, Kopanchuk S, Tobi A, Kilk K, Saalik P, Kurm K, Squadrito ML, Kotamraju VR, Rinken A, De Palma M, Ruoslahti E, Teesalu T, Sci Rep 2017, 7, 14655. [PubMed: 29116108]

[34]. Fogal V, Zhang L, Krajewski S, Ruoslahti E, Cancer Res 2008, 68, 7210; [PubMed: 18757437] Laakkonen P, Porkka K, Hoffman JA, Ruoslahti E, Nat Med 2002, 8, 751. [PubMed: 12053175]

[35]. Ruoslahti E, Adv Drug Deliv Rev 2017, 110–111, 3.

[36]. Feron O, Sci Transl Med 2010, 2, 34ps26;Liu X, Jiang J, Ji Y, Lu J, Chan R, Meng H, Mol Syst Des Eng 2017, 2, 370; [PubMed: 30498580] Sugahara KN, Teesalu T, Karmali PP, Kotamraju VR, Agemy L, Girard OM, Hanahan D, Mattrey RF, Ruoslahti E, Cancer Cell 2009, 16, 510. [PubMed: 19962669]

[37]. Keller AA, Maess MB, Schnoor M, Scheiding B, Lorkowski S, Methods Mol Biol 2018, 1784, 187; [PubMed: 29761400] Maeß MB, Wittig B, Lorkowski S, Journal of visualized experiments: JoVE 2014, e51960. [PubMed: 25226503]

[38]. Mitra AK, Davis DA, Tomar S, Roy L, Gurler H, Xie J, Lantvit DD, Cardenas H, Fang F, Liu Y, Loughran E, Yang J, Sharon Stack M, Emerson RE, Cowden Dahl KD, Barbolina VM, Nephew KP, Matei D, Burdette JE, Gynecologic oncology 2015, 138, 372. [PubMed: 26050922]

[39]. Bartlett DW, Davis ME, Nucleic acids research 2006, 34, 322. [PubMed: 16410612]

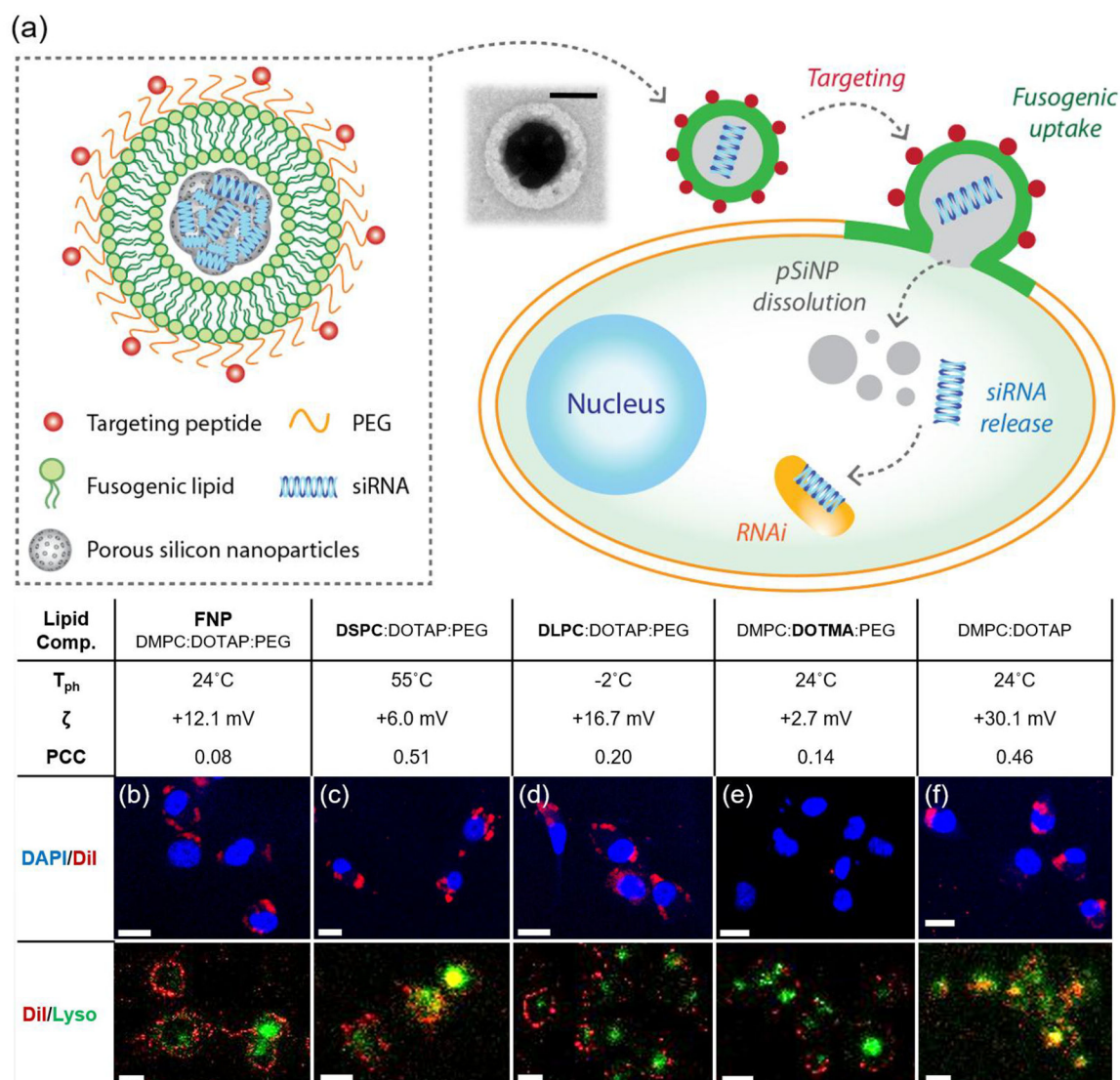[40]. Draz MS, Fang BA, Zhang P, Hu Z, Gu S, Weng KC, Gray JW, Chen FF, Theranostics 2014, 4, 872. [PubMed: 25057313]

Lipid Comp.	FNP DMPC:DOTAP:PEG	DSPC:DOTAP:PEG	DLPC:DOTAP:PEG	DMPC:DOTMA:PEG	DMPC:DOTAP
T_{ph}	24°C	55°C	-2°C	24°C	24°C
ζ	+12.1 mV	+6.0 mV	+16.7 mV	+2.7 mV	+30.1 mV
PCC	0.08	0.51	0.20	0.14	0.46

Figure 1. Fusogenic nanoparticles (FNPs) are able to deliver payloads directly into the cytoplasm by fusion with the cellular plasma membrane.

(a) Schematic of FNP structure and hypothesized uptake pathway in cells. pSiNP stands for porous silicon nanoparticles, siRNA represents a double stranded RNA construct, RNAi stands for ribonucleic acid interference, and PEG is a polyethylene glycol oligomer. Inset shows transmission electron microscope image of FNPs with 2% uranyl acetate negative staining. Scale bar represents 100 nm; **(b-f)** confocal microscope images showing the effect of replacing various lipid constituents on the ability of the nano-constructs to infiltrate CAOV-3 cells: **(b)** FNPs, the optimized lipid formulation used in this study; **(c)** DMPC replaced with DSPC; **(d)** DMPC replaced with DLPC; **(e)** DOTAP replaced with DOTMA; and **(f)** elimination of DSPE-PEG. For these experiments no targeting peptide was used; instead, the terminus of the PEGylated lipid component was methoxy (mPEG) rather than a peptide. All formulations contained the DiI membrane dye in the lipid coat, and cells were stained with either DAPI nuclear stain or the LysoTracker Green lysosomal compartment stain ("Lyso"). Scale bar represents 10 μm.
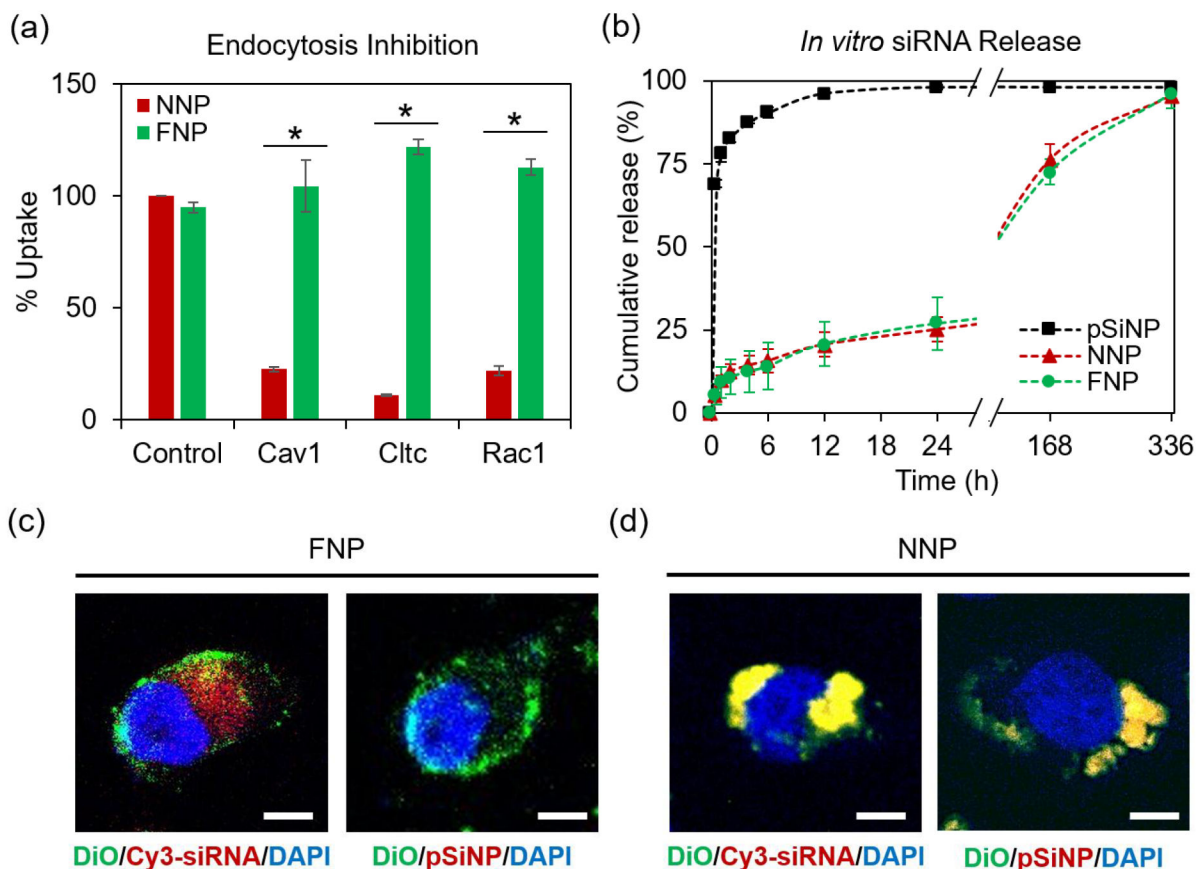
Figure 2. Lipid coating of FNPs protect siRNAs from leakage, and allow for cytosolic release upon fusion and pSiNP degradation.
(a) Uptake quantification of DiI-loaded FNPs and NNPs administered to CAOV-3 cells that were depleted of major markers of endocytosis (*cav1, cltc, rac1*); **(b)** *in vitro* cumulative release over time of siPI3Kγ from pSiNPs (porous silicon nanoparticles loaded with siPI3Kγ without lipid coating), NNPs (non-fusogenic nanoparticles loaded with siPI3Kγ), and FNPs (fusogenic nanoparticles loaded with siPI3Kγ). Cumulative release measured by siRNA absorbance measured in the supernatant after centrifugal separation of nanoparticles. Error bars represent n=6; **(c)** confocal microscope images of CAOV-3 cells treated with FNPs. Left panel shows cells treated with FNPs loaded with lipophilic DiO (green) in the lipid shell and cy3-siIRF5 (red) in the porous silicon core. Right panel shows cells treated with FNPs loaded with lipophilic DiO (green) and (non-labeled) siIRF5-loaded porous silicon core (red indicates intrinsic photoluminescence from the Si core); **(d)** confocal microscope images of CAOV-3 cells treated with NNPs. Left panel shows cells treated with NNPs loaded with lipophilic DiO (green) in the lipid shell and cy3-siGFP (red) in the porous silicon core, and right panel shows cells treated with NNPs loaded with lipophilic DiO (green) and siGFP-loaded porous silicon core (red indicates intrinsic photoluminescence from the Si core). Error bars represent standard deviation of n=6; Scale bar represents 5 μm.
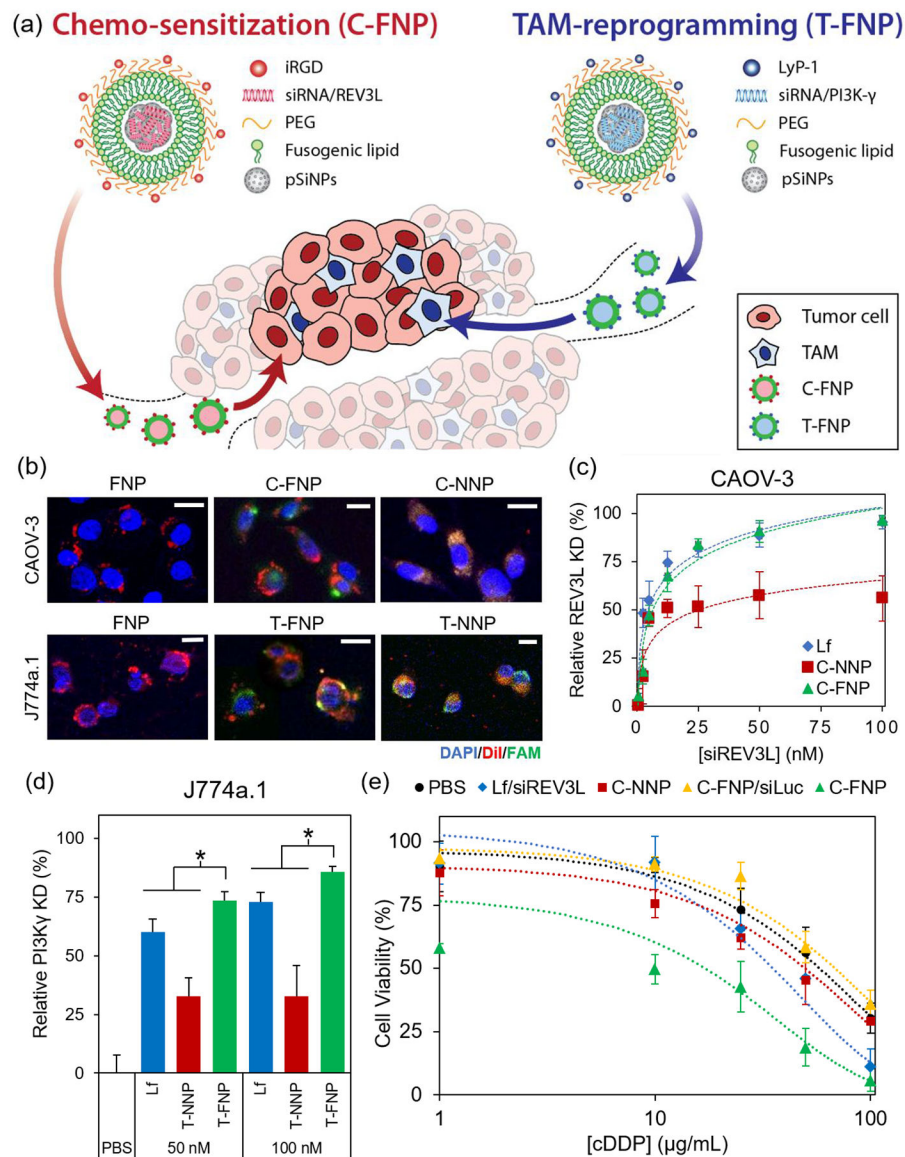
Figure 3. FNPs induce potent gene silencing effect *in vitro* and can sensitize cancer cells to chemotherapy.

(a) Schematic showing intended mode of action of the two formulations. The chemo-sensitizing fusogenic nanoparticles (C-FNPs) are loaded with siRNA against *Rev3l* and are targeted to cancer cells *via* the iRGD peptide, and the TAM-reprogramming fusogenic nanoparticles (T-FNPs) are loaded with siRNA against *Pi3kγ* and are targeted to TAMs *via* the LyP-1 peptide; **(b)** confocal microscope images of CAOV-3 cancer cells (top row) and J774a.1 macrophages (bottom row) treated with DiI-loaded FNPs or non-fusogenic NNPs that were non-targeted (FNPs), targeted with iRGD (C-FNPs and C-NNPs) or with LyP-1 (T-FNPs and T-NNPs). The peptides were tagged with FAM (green in the images) and cell nuclei were stained with DAPI (blue). Red channel is the DiI membrane dye. Scale bar represents 10 μm; **(c)** dose-response curve of CAOV-3 cells treated with increasing doses of siRNA against *Rev3l* using Lipofectamine (Lf), iRGD-conjugated non-fusogenic particles (C-NNPs), or iRGD-conjugated fusogenic particles (C-FNPs). Bars represent standard

deviation with n=8; **(d)** *Pi3kγ* knockdown quantification in J774a.1 macrophages treated 50 or 100 nM of siRNA against *Pi3kγ* using Lipofectamine (Lf), LyP-1-conjugated non-fusogenic particles (T-NNPs), or LyP-1-conjugated fusogenic particles (T-FNPs). Bars represent standard deviation with n=8. *represents p<0.05 using One-way ANOVA with Tukey HSD test; **(e)** chemosensitivity test in CAOV-3 cells with *Rev3l* silencing using PBS, Lipofectamine with siRNA against *Rev3l* (Lf/siREV3L), C-NNPs, C-FNPs with siRNA against luciferase, and C-FNPs. Cells were treated with increasing doses of cisplatin (cDDP) as indicated. Bars represent standard deviation with n=10.
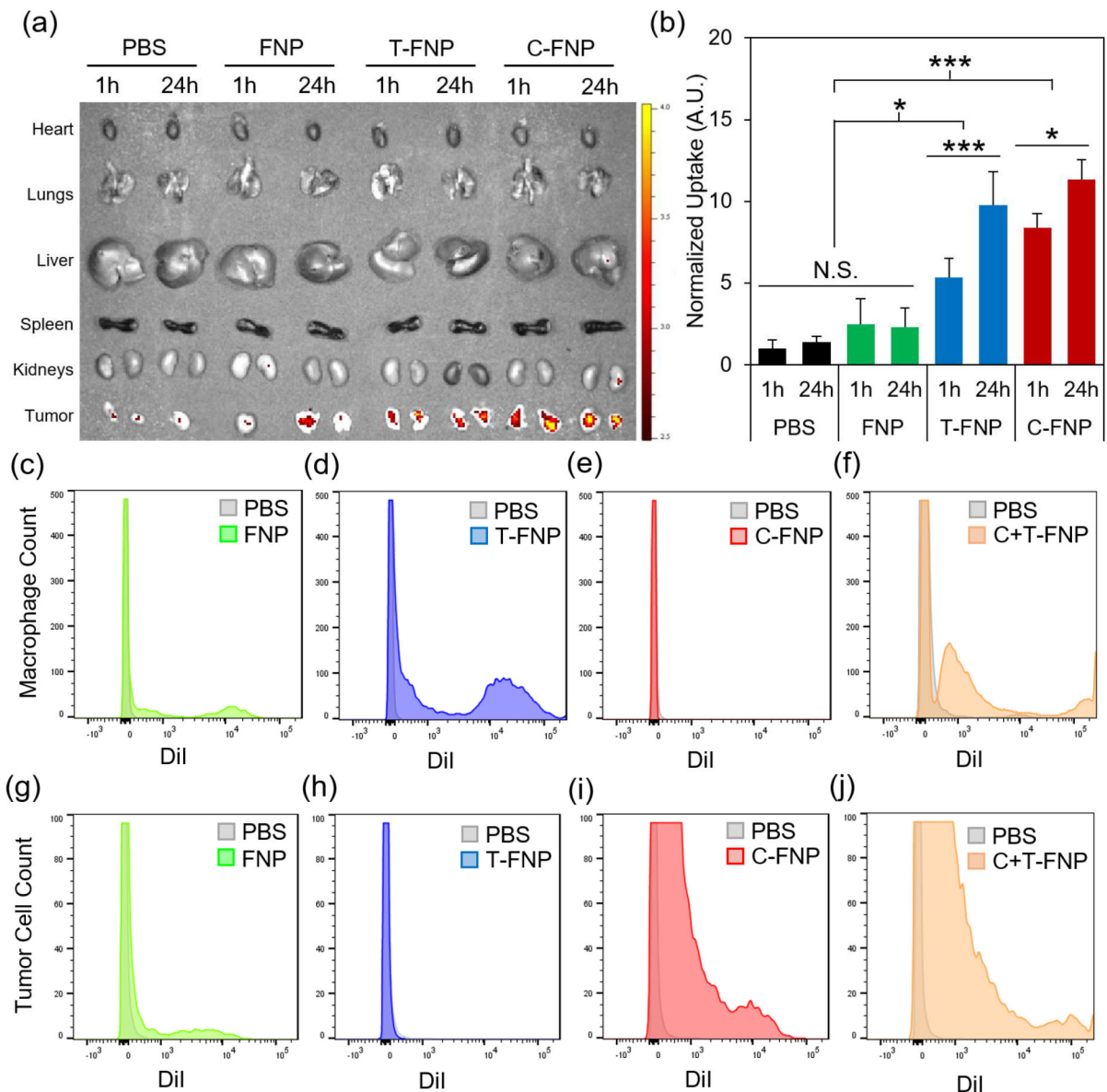
Figure 4. T- and C-FNPs selectively home to their target cells *in vivo* with minimal off-target accumulation.

(a) *ex vivo* IVIS 200 fluorescence images of organs harvested from mice bearing peritoneal carcinomatosis of CAOV-3 cells. Mice were IP-injected with PBS, DiI-loaded non-targeted FNPs, DiI loaded LyP-1 conjugated T-FNPs (fusogenic nanoparticles targeted to tumor associated macrophages, or TAMs, via the LyP-1 peptide), and DiI-loaded iRGD-conjugated C-FNPs (chemosensitizing fusogenic nanoparticles, targeted to tumor cells via the iRGD peptide) for 1h or 24h accumulation time. Image representative of n=5; **(b)** Image J quantification of DiI fluorescence signals from IVIS 200 images. Bars represent standard deviation with n=5. * represents One-way ANOVA with Tukey's HSD test with p<0.05, *** represents the same with p <0.01, and N.S. represents no significance; **(c-j)** DiI signal quantification using flow cytometry of macrophages purified from IP lavage fluid and tumor nodule homogenates **(c-f)**, or tumor cells **(g-j)** from the nodule homogenates. Samples were

harvested from mice IP injected with DiI loaded FNPs, T-FNPs, C-FNPs, or a 1:1 cocktail of C- and T-FNPs. Data is representative of n=4.
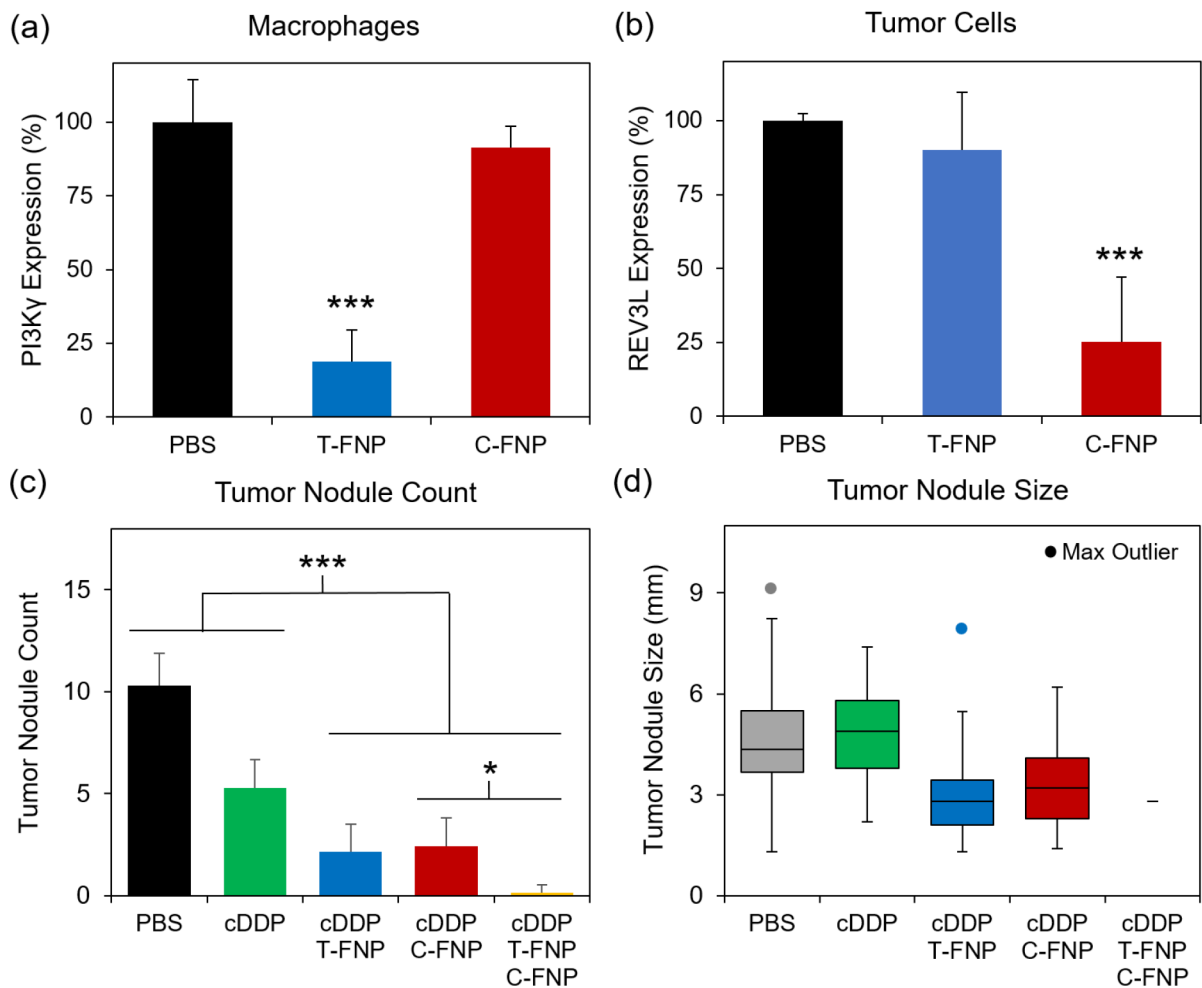
Figure 5. T- and C-FNPs are effective as immuno- and gene therapy formulations for combination treatment with chemotherapy.

(a) *Pi3kγ* expression quantified in macrophages purified from IP lavage fluid and tumor nodule homogenates using qRT-PCR. Mice bearing CAOV-3 human ovarian adenocarcinoma tumors were IP injected with PBS, LyP-1 conjugated FNPs carrying siRNA against *Pi3kγ* (T-FNP), or iRGD conjugated FNPs carrying siRNA against *Rev3l* (C-FNP). Bars represent standard deviation with n=6. *** represents One-way ANOVA with Tukey's HSD test with $p < 0.01$; (b) *Rev3l* expression quantified in tumor cells from tumor nodule homogenates using qRT-PCR. Mice were IP injected with PBS, T-FNP, or C-FNP. Bars represent standard deviation with n=6. *** represents One-way ANOVA with Tukey's HSD test with $p < 0.01$; (c) number of tumor nodules found in mice peritoneum after 30 days of treatment with PBS, cisplatin (cDDP) at 2 mg/kg, 1:1 cocktail of cDDP with T-FNPs, 1:1 cocktail of cDDP with C-FNPs, or 1:1:1 cocktail of cDDP, T-FNPs, and C-FNPs. Bars represent standard deviation with n=7. * represents One-way ANOVA with Tukey's HSD test with $p < 0.05$, and *** represents the same with $p < 0.01$; (d) size distribution of tumor nodules found mice from (c). Bars and boxes represent each quartile and dots represent

outliers, with $n_{PBS}= 72$, $n_{cDDP}= 37$, $n_{cDDP+T-FNP}= 15$, $n_{cDDP+C-FNP}= 17$, and $n_{cDDP+T-FNP+C-FNP}= 1$.